# Design of an expert distance metric for climate clustering: The case of rainfall in the Lesser Antilles

Emmanuel Biabiany, Didier Bernard, Vincent Pagé, Helene Paugam-Moisy

# Design of an expert distance metric for climate clustering: the case of rainfall in the Lesser Antilles

Emmanuel Biabiany[a,b,*,1], Didier C. Bernard[a,**,2], Vincent Page[b,2] and Hélène Paugam-Moisy[b,3]

[a]Laboratoire de Recherche en Géosciences et Énergie, Université des Antilles, Guadeloupe
[b]Laboratoire de Mathématique, Informatique et Applications, Université des Antilles, Guadeloupe

ARTICLE INFO

*Keywords*:
Machine Learning
Data processing
Clustering
Image Processing
Tropical Rainfall
Lesser Antilles

ABSTRACT

To expand our knowledge of the climate in the Lesser Antilles, we attempted to identify the spatio-temporal configurations of daily weather. We noticed certain pitfalls that can lead to poor results when using clustering algorithms and have proposed some steps towards the solution. These advancements might prove interesting for climate informatics, as well as for many applications that cluster physical fields. We illustrated the pitfalls with a dataset of cumulative rainfall from NASA's Tropical Rainfall Measuring Mission for the period 2000 to 2014. First, the pitfall is the lack of numerical evaluation of the clusters found by the algorithms, which prevents the comparison of algorithms. We used silhouette index for this evaluation and to demonstrate other problems. Second, algorithms like K-means cluster the points around their barycentre. For many physical fields, this barycentre is trivial, which may lead to poor performances. Third, the L2 norm used in conventional clustering methods, such as K-means and hierarchical agglomerative clustering, focus on the exact location of fields, which leads to poor evaluations of similarity between fields. We replaced it by a similarity measure called the expert distance (ED) that compares the histograms of four zones, based on the symmetrised Kullback–Leibler divergence. It integrates the properties of the observed physical parameter and climate knowledge. With these improvements, the results revealed five clusters with high indexes. The algorithms now discriminate the daily scenarios favourably, thereby providing more physical meaning to the resulting clusters. The interpretation of these clusters as weather types is discussed.

## 1. Introduction

The automatic identification of spatio-temporal structures that are indicative of the atmosphere's low frequency variability has long been known as an important research objective (Michelangeli et al. (1995); Burlando (2009); Kaufman and Roussew (1990); Ayrault et al. (1995); Ghil and Robertson (2002); Jury and Malmgren (2012)). Called weather types (WTs), these structures can be recurrent, nearly stationary (Michelangeli et al. (1995); Brunet and Vautard (1996)), and have their own identity (Vautard (1990)). The approach used in all these studies (except for Jury and Malmgren (2012) that will be discussed later), is as follows: for a selected physical parameter, a day is characterised by a spatial field that can be visualised as a map. The days that constitute the database are processed by a clustering method that creates clusters of similar days (Tian et al. (2014); Hadzimejlic et al. (2013); Monteleoni et al. (2013)). The average (named centroid) of each cluster of days is considered to be a WT. The two methods of clustering commonly

*Corresponding author
**Principal corresponding author
emmanuel.biabiany@univ-antilles.fr (E. Biabiany); didier.bernard@univ-antilles.fr (D.C. Bernard); vincent.page@univ-antilles.fr (V. Page); helene.paugam-moisy@univ-antilles.fr (H. Paugam-Moisy)
ORCID(s): 0000-0003-2934-5291 (E. Biabiany); 0000-0001-7531-3528 (D.C. Bernard)
[1]Developement of main algorithm implementation, manuscript writing and reviewing.
[2]Conceptualization of the work, supervisory guidance, manuscript writing and reviewing.
[3]Supervisory guidance and manuscript reviewing.

used to process climate clustering data are the K-Means (KMS) and Hierarchical Agglomerative Clustering (HAC) methods (Tian et al. (2014)).

All these articles share another common point, namely, the absence of a numeric evaluation of the clusters' quality. The evaluation of the clusters' quality can be carried out with a multiplicity of considerations, ranging from the physical plausibility of the centroids of the resulting clusters, intra class and extra class variance, and analysis of the temporal distribution of the clusters' days to deduce the composition of the seasons in terms of WTs (Chadee and Clarke (2015)). Some authors (Moron et al. (2016)) chose to establish correlations with other physical parameters to evaluate the reliability of these clusters. All these considerations make sense when it comes to the physical analysis of the climate, but such multiplicity hinders the comparisons among methods.

In contrast, we resort mainly to a single performance measure in this study (namely, the silhouette index, Rousseeuw (1987)) and reveal the major flaws with traditional clustering methods. Specifically, our results indicate that they do not produce relevant clusters. To confirm this assertion, we illustrated that these clusters are characterised by a low homogeneity (producing clusters that contain very distinct situations) and low separation (producing clusters faintly distinct from each other). When this point has been established, we analyse the origin of the problems with these methods, which have two main causes.

First, the use of L2 as a similarity measure between two spatial fields raises questions. We show that the distance L2, used to compare two days, does not show the following basic characteristic: the proximity of two days in the sense of the retained distance must be equivalent to the proximity between them from a physical point of view. To overcome this, we propose a pseudo-distance to cluster spatio-temporal rainfall fields. We provide a physical explanation for the principles that led to the definition of this pseudo-distance and show how incorporating it will enable further realistic results.

Second, the use of a field average of a cluster days (its centroid) as the main representative of a cluster (Jain (2008); Gokila et al. (2016)) also raises questions. The rainfall dataset used in this study has many spatial discontinuities that can probably explain the poor results obtained by traditional methods. All the previous researchers used algorithms like KMS that aggregate days around centroids on more continuous datasets. The majority of the studies describe the final centroids of the clusters as a WT. However, for the type of data used in this study, this is trivial because this average may not be the representative of an existing physical scenario. The pseudo-distance that we propose improves this phenomenon when clustering.

To describe the resulting clusters, we present the most representative days of each cluster (not an average), which seem to be more relevant endpoint. These clusters are related to the WTs and circulation types (CTs) presented in the previous study. We consider their intra- and interannual dynamics to understand their links with the seasons and the

interseasons. A specific analysis by island allowed us to understand the impact of these rainfall patterns on the Lesser Antilles, and we also compared satellite observation data (used for clustering) with data from ground rainfall stations.

The data used and the methodology developed are presented in section 2. Section 3 provides an evaluation of the results obtained for the study and a discussion of the important aspects of the results. It is divided into the following two parts: at first, we present a numeric comparison of methods, discuss our choices of parameters, and evaluate the quality of the resulting clusters to show that our method gives significantly better results than traditional methods; then, we provide a physical analysis by relating the clusters produced by this method to the existing knowledge on climatology in the Caribbean region. The last section is dedicated to the conclusions and perspectives.

## 2. Material and methods

### 2.1. Datasets

The study data consist of rainfall measured by the satellites of the Tropical Rainfall Measuring Mission (TRMM) Huffman et al. (2007). These data were spatialised with a grid of 0.25° longitude × 0.25° latitude. The geographic zone ranges from $-66.25$ to $-20.25° E$ and from 5 to $30° N$. It includes the Lesser Antilles islands along with the northeastern part of South America and a part of the Central Atlantic Ocean with the Cape Verde archipelago (cf Fig 1). Each day was thus represented by a field of $101 \times 187$ values, which were transformed into a vector of $18,887$ components. The data covered the period from 2000 to 2014, representing a base of $5,415$ days.

To determine recurring situations from the rainfall field, we used conventional clustering methods such as the HAC or KMS (Monteleoni et al. (2013); Rokach and Maimom (2010); Parmar and Saket (2017)). Notably, in the climate datasets, a field is a vector in a space with very large dimensions ($18,887$ pixels in our case), which made the search for relevant information relatively complex. To assess the study area, surface rainfall data supplied by Meteo France (Guadeloupe and Martinique) from 1979 to 2014 were used in the design of the expert distance (ED) (Section 2.4). To complete the analysis and interpretation of the clustering results, atmospheric circulation data at 850hPa from ERA-5 collected by radiosondes from *Wyoming Weather* from 1979 to 2014, and tropical storm and hurricane tracking data from 2000 to 2014 indexed on *Unisys Weather* were used (Section 3).

### 2.2. Clustering performance measures

As pointed out in Section 2.4, current publications in the field lack an important element, namely, they do not provide reliable, quantitative performance measures that indicate the quality of the resulting clusters. For example, in the article by Chadee and Clarke (2015), only the centroids of the clusters were evaluated and the clusters were considered to be correct because the centres were plausible and physically interpretable. However, the dispersion of

the clusters was not evaluated.

The absence of such quantitative quality measurements is particularly problematic when it comes in comparing the clustering methods. It is necessary to implement a way to measure the quality of the clusters, even if quality is recognised in the literature as a challenging problem, primarily in the cases where it is difficult to form hypotheses on the shape of the clusters searched for Tibshirani et al. (2001); Halkidi et al. (2001); Lallich and Lenca (2015).

In the absence of ground truth information, here is a list of some internal quality measurements that can be used with the clusters: the silhouette index (Rousseeuw (1987)), Calinski–Harabasz index (Caliski and Harabasz (1974)), and Davies–Bouldin index (Davies and Bouldin (1979)). All of them combine the following two essential qualities expected for clusters representing different physical situations: compactness (homogeneity) as well as distance (separation). We selected the silhouette index because it has the following benefits:

- It provides a quality measure for each day within its cluster, for each cluster, and for the method through all its resulting clusters,
- It is easy to interpret in terms of the pertinence of clusters.

Let us assume a clustering algorithm $\mathcal{M}_k$ that divides a dataset into $k$ clusters. At the end of the clustering process, each point $i$ of the data is assigned to a specific cluster $C_i$. The silhouette index $S(i)$ for each $i$ is obtained as follows:

$$S(i) = \frac{b(i) - a(i)}{max(a(i), b(i))}, \tag{1}$$

where $a(i)$ is the average of the distances between $i$ and the other elements in its cluster and $b(i)$ is the minimum of the averages of the computed distances between $i$ and the elements of every other cluster. In equations 2 and 3, $d(i, j)$ expresses the distance used to compare two elements $i$ and $j$, as shown below:

$$a_i = \frac{1}{|C_i| - 1} \sum_{j \in C_i, j \neq i} d(i, j), \tag{2}$$

and

$$b_i = min_{i \neq j} \frac{1}{|C_j|} \sum_{j \in C_j} d(i, j), \tag{3}$$

where $C_i$ is the cluster of $i$ and $|C_i|$ the size of $C_i$. By default, this distance $d(i, j)$ is the L2 norm. In this work, we

will replace the L2 distance with ED (Equation 9). Two other criteria may be estimated. The first, which indicates the average quality of a cluster $C_i$, can be calculated by using the following formula:

$$Sc(C_i) = \frac{1}{|C_i|} \sum_{j \in C_i} S(j). \tag{4}$$

In order to evaluate all of the clusters obtained by applying a clustering method $\mathcal{M}_k$ to our data, we can consider the average of each cluster's coefficients, namely:

$$Sa(\mathcal{M}_k) = \frac{1}{k} \sum_{i=1}^{k} Sc(C_i). \tag{5}$$

By definition, each coefficient is between $-1$ and 1. The coefficient reflects the combined evaluation of the proximity of an element to the elements of its cluster and the distance of this element to all the other clusters.
$Sa(\mathcal{M}_k)$ provides an indication of the quality of the result of a clustering method. For more information, readers can refer to Rousseeuw (1987). Here are some commonly accepted reference values that we will use later:

- values greater than 0.20 indicate good performance (existence of relevant and well separated clusters),
- values less than 0.10 indicate the opposite,
- negative values indicate that many points are assigned to clusters that do not represent the best possible choice.

## 2.3. Problems related to the L2 distance

All the work we were able to review in this domain uses the same distance measurement to compare two fields, namely, the distance associated with the L2 norm. For the record, this distance between two vectors of daily data $D_1(v_1, v_2, .., v_n)$ and $D_2(v_1, v_2, .., v_n)$ is calculated as follows:

$$d_{L2}(D_1, D_2) = \sqrt{\sum_{i=1}^{n} (D_1(v_i) - D_2(v_i))^2}, \tag{6}$$

where $D_x(v_i)$ is the $i$-th value $v$ of the vector of daily data $D_x$ and $n$ is the length of vectors of daily data. This distance seems to be partly responsible for the difficulties encountered by the clustering methods in the field of climate informatics Monteleoni et al. (2013). Figure 2(a) shows this property schematically, in which the distance L2 found between the reference (in black) and the two fields is the same. In addition, for fields such as rainfall, which show

extensive spatial and temporal irregularities, a day $D_1$ with a low spatial disparity relative to the reference (Fig 2(b)) will have a norm L2 equivalent to a day $D_2$, red curve, with a bigger spatial disparity. Thirdly, when data are described in a large vector space, a multitude of small fluctuations that are spatially spread across the field can be considered as important as one single big and very localised fluctuation.

## 2.4. Design of the expert distance

In this section, as with other authors in different application fields before (Pandit and Gupta (2011); Parmar and Saket (2017); Gibbs and Su (2002); Shraddha and Suchita (2011)), we propose an alternative similarity measure based on the fact that the correction, even slight, of L2's biggest weaknesses should result in significant improvements. The construction of the proposed measure will reduce the influence of the spatial location by a suitable subdivision and a quantification.

### *2.4.1. Partial management of spatialization*

For several computer vision applications, the image can be analysed at the patch level rather than at the individual pixel level (Barnes et al. (2011); Dinu et al. (2012); Amelio and Pizzuti (2016)). Image patches contain contextual information and have advantages in terms of computations and generalisations (Guo and Dyer (2007)). From this point of view, the decomposition of an image into patches or zones that do not overlap provides a simple but effective way of overcoming the curse of dimensionality (Xin (2017)).

In this study, we subdivided the rainfall field of the North Atlantic tropical zone into four patches (Fig 1) to limit the computation time and demonstrate the value of the approach without seeking to optimise it. The definition of these zones serves an important purpose, namely, to take the knowledge of field experts into consideration. Thus, each zone corresponds to a specific and known centre of action. In Fig 1, A1 is the zone in which the cold surges originate; A2 is the North Atlantic Subtropical High (NASH) zone; A3 is influenced by the continental zone and the arc of the Lesser Antilles; and A4 is the zone of low pressure that is linked to the presence of the Intertropical Convergence Zone (ITCZ). To compare two fields, we subdivided the fields according to these four zones and then compared each of them with their correspondent.

### *2.4.2. Comparison of the distribution of intensities*

Once each field had been spatially subdivided, we no longer had to pinpoint the exact location of the phenomena in each zone. It seems relatively reasonable to ignore their position down to the exact mesh, and instead we looked at the distribution of the rainfall intensities of the observed field, ignoring the notion of spatial location. In the absence of knowledge of the form of the distribution of rainfall intensities, the Kullback–Leibler divergence appears to be a

judicious choice (Kwitt and Uhl (2008); Kullback and Leibler (1951); Walker et al. (2004)). It is expressed as follows:

$$D_{KL}(P,Q) = \sum_{c} P(c) log \frac{P(c)}{Q(c)}, \tag{7}$$

where $P$ and $Q$ are two distributions of discrete probabilities and c is the index of possible values taken from each distribution. To obtain a metric for $\mathbb{R}_+$ that also has the symmetry property, we will use the symmetrised divergence of Kullback–Leibler, namely:

$$D_{KLS}(P,Q) = D_{KL}(P,Q) + D_{KL}(Q,P). \tag{8}$$

Although it is possible to define a measure of the Kullback–Leibler divergence adapted to continuous fields, we preferred to quantify the data differently because estimating the probability densities of the intensities raises parametrisation problems. Moreover, such quantification might help to reduce the effects of the small fluctuations noted in Section 2.3, even though edge effects around the boundaries of the selected intensity classes remain. The histogram bins were determined from the rainfall data collected in the area. We selected eight bins of possible intensities. The boundaries of these bins were selected from the rainfall data collected in the area such that the distribution of the bins was uniform (cf. Table 1).

The distinct intensity distributions obtained were then used to compute the Kullback–Leibler divergence in each zone. The average of the divergences by zone provides the distance between two days. We call this the expert distance, which is referred to as ED, and the quantity is defined by:

$$ED(D_1, D_2) = \frac{1}{n} \times \sum_{i=1}^{n} D_{KLS}(D_1 Z_i, D_2 Z_i), \tag{9}$$

where $D_1$ et $D_2$ are days and $D_x Z_i$ is the histogram of the zone with reference $i$. In our case, the number of zones $n$ equals four as presented in Fig 1. All the operations listed above are summarised in Fig 3.

## 3. Results and discussion

In this section, we present the results and discuss the results at first from a computer science point of view. The last subsection will be dedicated to an analysis of the results for the specific application considered.

### 3.1. Performance measurements of clustering methods

We used algorithms such as HAC and KMS with which we separately linked L2 and ED. To reveal the possibilities of using these two distances, the evaluation of the quality of the clusters obtained by HAC-L2, KMS-L2, HAC-ED, and KMS-ED was performed by computing the silhouette coefficients (Equation 5). Figure 4 shows the evolution of the silhouette coefficient as a function of the number $k$ of clusters.

The results showed several interesting points for the comparison between KMS and HAC, which are summarised below. Notably, the methods based on the HAC algorithm produced coefficients that were significantly lower than those obtained by KMS algorithms. Additionally,

- For HAC-ED, the silhouette coefficient approached 0 for $k > 3$, thus indicating the irrelevance of the clusters detected.
- HAC-L2 exhibited negative silhouette coefficients, thus indicating that the points were affected by suboptimal clusters.
- HAC-ED produced results superior to HAC-L2, although the performance of both remained very weak.

We can now eliminate the HAC algorithms and focus on KMS. This choice is in line with the literature Chadee and Clarke (2015), in which HAC has been used only to define the initial centroids of the KMS algorithm by ruling out any random selection of these centroids. Here,

- KMS-ED largely outperformed KMS-L2.
- KMS-ED exhibited values mainly over 0.2 for a significant number of clusters, thus indicating the presence of relevant structures within the data.
- KMS-L2 exhibited values under 0.1 for $k > 2$, thus indicating irrelevant clusters.
- Although the shape of the curves generally decreased with $k$, a slight inflection was observed around $k = 5$ in both cases.
- For this value of $k = 5$, KMS-L2 had a silhouette value of 0.08, whereas KMS-ED had a value of 0.26.

The selection of the optimal $k$ was not as clear-cut as we had hoped, in spite of the noted inflection around $k = 5$ in both cases. This led us to choose this number of clusters for the following analyses. When considering large maritime areas with little land surface, such as the Caribbean region (Fig 1), according to authors of earlier works Vigaud and Robertson (2017); Moron et al. (2016); Chadee and Clarke (2015); Sáenz and Durán-Quesada (2015), the number of WTs obtained by using KMS or HAC can range from 7 to 11. Hence, five WTs seems a bit low in regard to the literature.

## 3.2. Visual inspection of the clusters found

For the present time, we have relied on the silhouette index for our analysis. Let us now show how the values of the silhouette index are relevant in terms of quality of the resulting clusters. Accordingly, we will carry out a detailed inspection of the clusters found by the KMS-L2 and KMS-ED methods with $k = 5$.

### *3.2.1. Illustration of irrelevant clusters*

The silhouette index results for KMS-L2 were indicative of irrelevant clusters ($< 0.1$). We can conclude that the L2 norm does not evaluate the similarity of spatial patterns of rainfall data properly and this leads to the aggregation of different situations in the same cluster, as illustrated in Fig 5(a). For the same reason, the method separates situations that are indeed very similar into different clusters, as seen on Fig 5(b). We precisely introduced the new similarity measure ED to overcome this flaw.

### *3.2.2. Illustration of the irrelevance of centroids for L2*

As stated before, the centroids have a major role in KMS algorithms, and some author rely on them to describe the Weather Types extracted by their algorithms. The idea behind this is that these averaged fields are representative of the clusters. Fig 6 show why we believe this idea should be discarded when dealing with discontinuous fields such as rainfalls. It shows, for a specific cluster found by KMS-L2, the centroid (Fig 6(a)), the nearest day to the centroid (Fig 6(b)) and a random day of the same cluster (Fig 6(c)).

This figure shows the following interesting aspects. The centroid does not look like any of the members of the cluster considered. We think that computing the average tends to create continuous artificial zones, which gives a bad spatial appreciation of the existing meteorological structures and leads to poor results for the clustering of spatio-temporal rainfall fields using L2. This problem can be partially avoided when using the ED as the centroid is now a distribution of rainfall in each region. These distributions are much more meaningful for describing rainfall situations. For the following analysis, we will consider, as a representative of the cluster, not the centroid but the most representative element of each cluster obtained. This is the element with the shortest distance to each cluster centroid (distance being L2 or ED in their respective cases).

### *3.2.3. Separation and homogeneity of the clusters*

As stated several times in this article, we prefer to rely on a single performance measure than on a multitude of considerations. We need, however, to prove that this performance measure is a good indicator of these considerations. This section is dedicated to the separation and homogeneity of the clusters.

#### *3.2.3.1. Separation*

To assess the **separation** of the clusters, Figs 7 and 8 show respectively the representative (see above) rainfall

fields of the clusters obtained by the KMS-L2 and KMS-ED methods for $k = 5$. These figures also show, for each representative field, the wind field of the corresponding day. This wind field has not been used during the clustering. It will be used in the physical analysis of the weather types extracted by our method, later in this article. Those representative fields (both rainfall and wind) should be as different as possible.

Figure 7 clearly shows that for KMS-L2, clusters C2 and C3 in fact depict situations that are quite similar with rainfall in the southeast. C1 and C5 are also similar and depict low rainfall across the space and an atmospheric circulation originating mainly from the northeast. The exact spatial location of these rainfall situations is the only thing that distinguishes them, thus illustrating precisely the limits of L2.

The results obtained for KMS-ED, shown in Fig 8, highlight, conversely, very diverse clusters. Each case shows centres that are more or less active.

#### *3.2.3.2. Homogeneity*

We also wanted to evaluate the **homogeneity** (the internal variability) of the clusters obtained for each method. Of these five clusters, for the sake of conciseness, we will present only one cluster per method. For each method. we selected the cluster whose $Sc(C_i)$ value (Equation 4) was the closest to the overall value of the corresponding method $Sa(\mathcal{M}_k)$. These were the C2 cluster for the KMS-L2 method and the C4 cluster for the KMS-ED method. The distance of each of the days composing a cluster to their representative was computed, and elements were sorted in ascending order. We extracted six quantiles from this ranking, to evaluate how each cluster varied internally. Fig 9 shows the quantiles obtained for KMS-L2. Fig 10 does the same for KMS-DE.

In the case of the L2 distance (Fig 9), the first three fields were relatively similar to the representative element, whereas the last two were different. In fact, on the central part and the northwestern edge, we found rainfall zones that were well localised. When grouping the results by the L2 distance, we observed a cluster of situations that were certainly similar in terms of numbers but very distinct from a physical point of view.

In the case of ED (Fig 10), the elements of cluster C4 had a certain physical constancy although they differed slightly in their visual appearance. This cluster consisted of low rainfall fields.

#### *3.2.3.3. Conclusion on the intrinsic quality of clusters*

The visual inspection confirmed the results observed by using only the silhouette index.

- KMS-L2 produced clusters of relative relevance, as some clusters representative were similar. Moreover, days among a cluster could be very different from a physical point of view.
- KMS-L2 produced more relevant clusters, which were reflective of diverse situations. Among a cluster, days

seemed similar.

From the point of view of the physical separation of the clusters, the introduction of the ED has clearly enabled the acquisition of clusters with a much higher relevance. In addition to the better results obtained by KMS-ED, this facet tends to reinforce that clusters with a high silhouette index are more relevant when it comes to their physical significance.

## 3.3. Physical analysis

As stated in the introduction, we wanted to pinpoint some pitfalls encountered when clustering daily fields in geoscience applications. We attempted to highlight them and present some partial solutions to these problems in the previous sections. This section will focus on the remarkable results obtained by our simple method as soon as these problems are dealt with. Our major goal was to extract typical geospatial structures of meteorological data, focussing only on rainfall. Some authors, like Jury and Malmgren (2012), have used several fields such as the surface temperature, sea-level pressure, and $U$ zonal wind to extract dominant modes with the help of a principal component analysis (PCA). While such a combined analysis of different fields is something we aim to do in the future, our article focusses on only one field (rainfall) to illustrate the general method we are proposing.

In our method, we chose to aggregate spatial areas in a controlled way (by using regions) to add as much physical knowledge as we could acquire in the design of the extraction of WTs. An interesting aspect of our study comes despite one of its limitations, namely, we treated each day independently and clustered days by taking no account of the time dependency between them, apart for the one found in the data themselves (this is a common approach).

We propose a physical analysis of the clusters obtained by looking at their intra- and interannual evolutions on a large scale. Then, we will continue the study of the meteorological comparability of daily precipitation at the local scale, including, in this case, surface observations.

### *3.3.1. Large scales*

#### *3.3.1.1. Annual variability and trends*

It is thus very interesting to observe the temporal distribution of the fields contained in each cluster to highlight possible annual and semi-annual cycles, as in Chadee and Clarke (2015). The frequencies were derived by applying the cluster analysis technique KMS-L2 and KMS-ED to the daily atmospheric precipitation patterns defined over the domain indicated in Fig 1. We also show the results of Mann–Kendall's nonparametric trend test (Yue et al. (2002)), which was performed on the annual frequencies of each group to test the null hypothesis of no trend at the 95% confidence level (5% significance level). Radiosonde parameters at different levels, such as specific humidity, wind direction, and intensity, were used to characterise the clusters. The days in each of the clusters would thus compare to several configurations in terms of outgoing longwave radiation (OLR), sea surface temperature (SST), and wind

circulation. We will try, as far as possible, to link them to the clusters found in previous study (Chadee and Clarke (2015); Moron et al. (2016); Martinez et al. (2019)).

For KMS-L2, the results are shown in Fig 11. On the left, we show the annual variability of the monthly frequencies of days making up each cluster, whereas the right side shows the inter-year change. Many of them have a similar annual distribution. Moreover, no significant trends over the 15 years of TRMM observations were found. This result confirms that the L2 distance is still not very appropriate for classifying daily rainfall fields, as it weakly reflects the seasonality effects for the TRMM daily rainfall.

For KMS-ED, Fig 12, the monthly distributions obtained were clearly separated because they better integrated regional physical and climatic knowledge. With this slight improvement, the results revealed five clusters ($k$=5) with high indexes ($Sa(M_k) > 0.2$), which can be characterised as follows :

- C1, represents 14.8% of the days analysed, with days spread over the whole 12 months, but data remained rather grouped over the first part of the year. The maximum was centred on the months of April and May. This cluster was associated with CTs 1 to 5 found in Chadee and Clarke (2015) and WTs 1 to 3, 7, and 8 found in Moron et al. (2016). There were no significant trends for the annual frequencies.

- C2 and C3, 12.5 and 10.4% respectively were close to each other because they were localised at the end of the year. However, for C2, the maximum matched with September–October, whereas for C3, this occurred in November. Decreases in the annual frequencies were found for C2 ($p$-value=0.02 and $r^2$=0.439), whereas there were no significant trends for C3. These clusters were associated with WTs 4,5,6, and 8 in Moron et al. (2016).

- C4 was the most prevalent type, in which it accounted for 32% of the days. The elements of this one were mainly distributed from December to April with a peak in February. It represents the cluster of the dry season. The annual distribution showed a marked “dip” between July and November (Fig 12). Figure 13 shows observations of the upper atmosphere at station 78897-TFFR Le Raizet. The daily precipitation fields of C4 showed a thin wet layer, which dried out at 800 hPa. In the lower levels, the trade winds were from the northeast, whereas for the levels below 500 hPa, the flow was predominantly from the northwest. In this case, the drivers, which are the NASH and the SST, limited the intensity of the observed rainfall (Davis et al. (1997); Dunion (2011); Moron et al. (2015)). The NASH and the North American High are connected together and provide strong diverging trade winds and subsidence in the Caribbean. The ITZC migrates southwards favouring the development of the southern flank of NASH (Martinez et al. (2019)). A detailed analysis of C4 indicated the presence of heavy precipitation. These conditions were related to cold fronts that managed to reach the low latitudes of the Lesser

Antilles (in January, April, and May). Indeed, at the interface between the two air masses, the trade winds carry a flow of warm, humid equatorial air, which intensifies convection and the development of active frontal cloud bands producing heavy rainfall Beucher (2010). The evolution of the number of days per cluster over the 15 years of TRMM observations showed a positive correlation, meaning an increase of C4 ($p$-value<0.022, $r^2$=0.342). This cluster can be associated with CTs 1 to 5 found in Chadee and Clarke (2015) and WTs 1 to 3, 7, and 8 found in Moron et al. (2016).

- C5, centred on July–August, was well separated from the dry season and contained the last third of the daily rainfall analysed. It represents the cluster of the rainy season with the highest contribution to the annual rainfall. For C5, unlike C4, the trade winds were established on a column of atmospheric air, which was higher and wetter (Fig 13). At this time of year, the NASH is moving northeast, which allows the more humid trade winds to flow to the east Caribbean due to the longer course over the Atlantic Ocean on its southeast flank. The Atlantic ITCZ reaches its northern most extent in the Lesser Antilles and begins its southward migration at this time (Martinez et al. (2019)). This period corresponds to the increase in convection with increased moisture advection in the Caribbean, which is favourable to higher daily precipitation (Jury and Malmgren (2012); Herrera and Ault (2017)). There was also a significant positive trend ($p$-value=0.028, $r^2$=0.321) which reflects an increase of C5 between 2000 and 2014 (Fig 12). C5 can be related to CTs 6–7 and WTs 4–6 found in Chadee and Clarke (2015) and Moron et al. (2016) respectively. Conflicting trade winds (shear lines), caused in this period by changes in wind direction and wind speed, passing from the northeast sector to the southeast sector resulted in heavy cloud cover and heavy rainfall. In addition, the close passages of the eastern waves triggered powerful updrafts with large areas of surface convergence favouring heavier rainfall on the eastern Antilles (Beucher (2010)).

Among the five retained clusters, C4 and C5 represent 62% of the sample, and these are the representative clusters of the bi-modal cycle. The remaining third was divided equally between C1, C2, and C3. Among the latter, some of the data may represent temporal transitions between seasons. These transitions may highlight differences between the northern and southern Caribbean. C2, C4, and C5 showed significant trends. The drying trend found for C4 also has been found by other authors over longer periods and prior to these TRMM observations (Jury (2009); Jury and Malmgren (2012); Jury and Bernard (2019)). The decrease in the number of C2 days over the last decade, combined with the increase in the number of C5 days, indicates a potential shift or even a tightening of the rainy season (Fig 12). For TRMM daily rainfall measured during these two periods, the increase in convection at the beginning and end of summer can be attributed to the oceanic and continental monsoon annual cycles (Jury and Malmgren (2012)). The latter has a positive influence on early summer rainfall but negative influence on late summer rainfall.

#### *3.3.1.2. Links to hurricanes season*

In our study regions, hurricanes are a major concern for resident populations and thus, it was of interest to analyse the distribution of hurricanes in clusters.

Tropical storms (TS) and hurricanes (H) recorded at the National Oceanic and Atmospheric Administration (NOAA) site from 2000 to 2014 helped us to attribute the different proportions of these types of atmospheric hazards to the clusters retained in KMS-ED. This work had not been done by Vigaud and Robertson (2017); Moron et al. (2016); Sáenz and Durán-Quesada (2015); Jury (2009); Jury and Malmgren (2012). The proportions are presented in Table 2. C2, C3, and C5 contained almost all of these hazards. The highest number of days with TS or H were found for C5, followed by clusters C2 and C3. These clusters included around 80% of the H and more than 90% of the TS. In relation to the size of the clusters, $P_{Cx}(H)$ in Table 2 results show a proportion twice as large (13%) of H in C2 as that of C5 (5.8%) and C3 (6.9%). C1 and C4 contained few hazards. However, in the previous subsection, these clusters have been identified as dry day clusters, but we did observe the presence of a few TS or H days. This seems to have been due to the fact that the NOAA database covers the central Atlantic Ocean and the whole Caribbean region. These phenomena are at the limit of our domain (Fig 1).

### *3.3.2. Local scales: Lesser Antilles of the east Caribbean*

In this paragraph we focus on the TRMM rainfall observed over the mountainous and flat islands of eastern Caribbean. Magnitude of rainfall across the Caribbean are affected by localized mechanism like orographic lifting or diurnal heating. They can enhance, to a lesser extent, convection to produce very different rainfalls between the windward and leeward parts in these islands (Jury and Bernard (2019)). In Figure 14, we have calculated the mean cumulative rainfall over all the meshes (occupying at least 20%) of the land surface, mean of spatial sum (MSS). The average per pixel of rainfall is represented by the mean of spatial mean (MSM). We also recorded the percentage of zeros included in each case (DWR).

These quantitative measures regrouped C1 and C4 (dry days), and C2 and C5 (rainy days), while C3 remained the intermediate cluster. The MSM results showed very different orders of magnitude, i.e. 5 to 7.5 *mm*/day for C2 and C5, 2 to 3.5 *mm*/day for C3, and 1.04 to 2.07 *mm*/day for C1 and C4. The MSS values of the islands of Dominica, Guadeloupe, and Martinique were the highest. Mountain ranges of these islands are real imposing barriers to the trade winds, which leads to orographic ascent of the humid air mass and precipitation. C1 and C4 had the highest DWRs on average, respectively between 34 and 60%, thus reflecting the presence of many days without precipitation in these clusters. For the flat islands, the values found were generally high but we believe there was bias due to the low surface area.

The histogram in Fig 15 compares TRMM to weather stations observations in Guadeloupe and Martinique. The TRMM data had overestimated pixels without rain and underestimated high rainfall. These results were found by Jury and Bernard (2019) for the cloudy peaks of this region. Biases reported here (e.g. low precipitation) could be related more to the peculiarities of the micro climate in steep topography than to the performance of model physics and data assimilation. However, it should be noted that rainfall between 8.7 to 16.4 *mm*/day is relatively well measured by the TRMM data.

Considering that the class 8.7–16.4 *mm*/day represents a moderate rainy day (well detected by TRMM), the Fig 16 shows the intra-annual ($y$-axis) frequency distribution for the analysed period ($x$-axis). The intra-annual evolution of this class over time showed good agreement between the local and regional scales. For the dry (C4) and wet (C5) seasons, the moderate rainfall class was almost evenly distributed with low frequencies. In the other three clusters, peaks with higher frequencies appeared but the distribution was more scattered (dispersed). From 2002 to 2011 C1, C2, and C3 showed punctually isolated maximums of moderate rainfall frequencies, which were observed from April to December. C1 seemed to be the cluster of the April–May inter-season, with its dry to rainy transition, and C3 appeared to be the cluster of the reverse transition during November–December.

# 4. Conclusion and perspectives

## 4.1. Conclusion

In this study, we used a similarity measure more suitable for the analysis of climate data for clustering tasks based on the Kullback–Leibler measure. This involved the design of a new metric, named the expert distance (ED), in which some knowledge of the meteorological structures derived from observational studies was considered, and we proposed a novel and unique strategy to strengthen the expected physical relevance. The unit data clustered were the daily rainfall data obtained by TRMM measurements on either side of the Lesser Antilles (the Atlantic Ocean and Caribbean Sea), and this was conducted to obtain the clusters of days with similar climate profiles.

We applied unsupervised classification methods (KMS or HAC) to discover global trends within the clusters. The analysis we performed by using these two methods encountered the following difficulties. First, as rainfall totals were widely scattered, “near” fields in the sense of L2 were rare; the L2 norm tended to agglomerate fields with a common spatial structure, although they were otherwise different. Additionally, the centroid used by KMS did not always represent a realistic physical situation.

Although the L2 norm is frequently used in climate data clustering, the results obtained herein were unsatisfactory, as the L2 standard did not effectively quantify the physical similarity between configurations. To better quantify the similarity of the daily rainfall, a spatial subdivision of fields was used. Once these patches were defined, we imple-

mented a pseudo-distance based on a relaxation of the precision of the spatial location of the fields, and we compiled histograms and compared them by using the Kullback–Leibler divergence. Similar concerns have already emerged in the field of retrieval image research, and we developed a subdivision technique suitable to our field corresponding to known precipitation drivers.

In addition, we used the silhouette index to evaluate the quality, coherence, and separation distance between the resulting clusters. We completed this analysis with a visual inspection of the clusters observed, which confirmed that expert deviation allows us to obtain improved results than the L2 standard when applied to this type of meteorological data. Five clusters, resulting from our best algorithm, were evaluated by experts.

Two main classes accounted for 62% of the daily totals, in almost similar proportions. For these, the monthly distribution and spatio-temporal averages were representative of the two predominant seasons at these latitudes, namely, the dry season and rainy season. These were focussed respectively on the months of February and August–September. Moreover, the interannual evolution revealed a significant increase in the number of constituent elements of these two clusters during the 15 years of measurements. There was a decrease in daily rainfall (drying), which was spread over the first four months of the year. Additionally, the rainy season seemed to be earlier as it moved towards the month of July. The spatio-temporal averages of the daily totals were 5–6 times greater for the mountainous islands.

Our study confirms the trends deduced by other bibliographical works. It also highlights certain small differences that have remained unattainable by classical clustering methods. The results obtained led to finer analysis details of the spatio-temporal dynamics of daily precipitation. Importantly, the analysed series was short and these results may evolve in accordance with increases in the observation period and improvements in the technologies used in the observation of rainfall by satellites, while remaining subjacent to the evolution of the climate.

The last third of the daily totals was rather representative of the transitions between the two main seasons. Two of them showed a more spread out intra-annual distribution of dry days, i.e. 14.8% of the total, followed by an average decrease in very rainy days in September–October. These results confirmed the drying trend in this region. With variable positioning and monthly durations, transitions were generally very difficult to identify. Only one of the clusters, 10.4% of the total, was representative of the transition from the rainy to dry season.

The new metric used represents a concrete step forward in the analysis of possible climatic and seasonal trends based on spatio-temporal data of daily rainfall. It offers good potential for identifying the dynamics of transitions, which often herald the possible severity of the two main seasons.

This study was based on a collaboration between physicists and computer scientists interested in the methods of data mining from large databases obtained either from satellite observations or computed as in the case of meteorological reanalyses.

The extracted clusters, from a climate physicist point of view, were characterised by relevance, if not originality. However, we believe that this method adds more finesse and accuracy in the analysis of the fields for a reasonable number of clusters.

### 4.2. Perspectives

We presented an approach that should be widely relevant to the present scope of Climate Informatics, as our observations remain valid for any application that uses the clustering of fields. However, as our goal was the extraction of weather types, we focus on these perspectives in future.

At first, we could do the exact same study for other single parameters, such as the wind or temperature, with the benefit that we can knowingly compare the quality of the clusters found for each parameter, itilizing silhouette index. Hence, it is possible to select the parameters that give better clusters and probably show that some parameters are irrelevant in the study of weather types in the Lesser Antilles.

Interestingly, we might, with small adjustments, combine parameters to extract clusters of days by relying on a diverse and more complete information. We can evaluate such data with a couple or several parameters to obtain potentially better clusters.

Furthermore, some parameters (for example, wind) might explain a phenomenon (for example, rainfall). Such an analysis is now possible by clustering the days according to a parameter (wind) and evaluating the quality of the cluster according to the explained phenomenon (rainfall). Employing silhouette index, we should be able to select the best parameter for a given phenomenon.

## Computer code availability

The algorithm presented in this work and developed by Emmanuel Biabiany, is called "dePrecitTRMM", implemented in GNU Octave (an alternative open-source of Matlab), and hosted at https://github.com/ebiabiany/expert-distance-precipitation with all the dependencies. Please note that the whole computation (including data pre-formatting, clustering and silhouette index calculation) takes about 48 hours, on a standard computer with an 8-core processor and 32 GB RAM.

## Acknowledgements

This research was supported by the Claude Emmanuel Blandin Foundation's research and FEDER&FSE 2014-2020 project intitled Changement Climatique et Conséquences sur les Antilles Françaises (https://c3af.univ-montp3.fr/).

## Data availability

Satellite measured precipitation daily products are available on NASA's TRMM project website (https://pmm.nasa.gov/data-access/downloads/trmm). ERA5 hourly data on pressure levels for wind components are aviable on Copernicus Climate webservice (https://cds.climate.copernicus.eu/cdsapp#!/dataset/reanalysis-era5-pressure-levels).

## References


Amelio, A., Pizzuti, C., 2016. A patch-based measure for image dissimilarity. Neurocomputing 171, 362–378. doi:https://doi.org/10.1016/j.neucom.2015.06.044.

Ayrault, F., Lalaurette, F., Joly, A., Loo, C., 1995. North atlantic ultra high frequency variability. Tellus A 47, 671–696. doi:10.1034/j.1600-0870.1995.00112.x.

Barnes, C., Goldman, D.B., Shechtman, E., Finkelstein, A., 2011. The patchmatch randomized matching algorithm for image manipulation. Commun. ACM 54, 103–110. doi:10.1145/2018396.2018421.

Beucher, F., 2010. Météorologie tropicale: des alizés au cyclone. Number vol. 2 in Cours et manuels - Direction de la météorologie, La Documentation Française. URL: https://books.google.gp/books?id=PNhDYgEACAAJ.

Brunet, G., Vautard, R., 1996. Empirical normal modes versus empirical orthogonal functions for statistical prediction. Journal of the Atmospheric Sciences 53, 3468–3489. doi:10.1175/1520-0469(1996)053<3468:ENMVEO>2.0.CO;2.

Burlando, M., 2009. The synoptic-scale surface wind climate regimes of the mediterranean sea according to the cluster analysis of era-40 wind fields. Theoretical and Applied Climatology 96, 69–83. doi:10.1007/s00704-008-0033-5.

Caliski, T., Harabasz, J., 1974. A dendrite method for cluster analysis. Communications in Statistics 3, 1–27.

Chadee, X.T., Clarke, R.M., 2015. Daily near-surface large-scale atmospheric circulation patterns over the wider caribbean. Climate Dynamics 44, 2927–2946. doi:10.1007/s00382-015-2621-2.

Davies, D.L., Bouldin, D.W., 1979. A cluster separation measure. IEEE Trans. Pattern Anal. Mach. Intell. 1, 224227.

Davis, R.E., Hayden, B.P., Gay, D.A., Phillips, W.L., Jones, G.V., 1997. The north atlantic subtropical anticyclone. Journal of Climate 10, 728–744. doi:10.1175/1520-0442.

Dinu, L.P., Ionescu, R.T., Popescu, M., 2012. Local patch dissimilarity for images, in: Huang, T., Zeng, Z., Li, C., Leung, C.S. (Eds.), Neural Information Processing, Springer Berlin Heidelberg, Berlin, Heidelberg. pp. 117–126.

Dunion, J.P., 2011. Rewriting the climatology of the tropical north atlantic and caribbean sea atmosphere. Journal of Climate 24, 893–908. doi:10.1175/2010JCLI3496.1.

Ghil, M., Robertson, A.W., 2002. "waves" vs. "particles" in the atmosphere's phase space: A pathway to long-range forecasting? Proceedings of the National Academy of Sciences 99, 2493–2500. doi:10.1073/pnas.012580899.

Gibbs, A.L., Su, F.E., 2002. On choosing and bounding probability metrics. International Statistical Review 70, 419–435. doi:10.1111/j.1751-5823.2002.tb00178.x.

Gokila, S., Ananda Kumar, K., Bharathi, A., 2016. Different versions of k-mean clustering in complete set of numerical data points. International Journal of Scientific Engineering and Applied Science 2.

Guo, G., Dyer, C.R., 2007. Patch-based image correlation with rapid filtering, in: 2007 IEEE Conference on Computer Vision and Pattern Recognition, pp. 1–6. doi:10.1109/CVPR.2007.383373.

Hadzimejlic, N., Donko, D., Hadzimejlic, N., 2013. Climate data analysis using clustering data mining techniques. Latest Trends in Applied Informatics and Computing .

Halkidi, M., Batistakis, Y., Vazirgiannis, M., 2001. On clustering validation techniques. Journal of Intelligent Information Systems 17, 107–145.

Herrera, D., Ault, T., 2017. Insights from a new high-resolution drought atlas for the caribbean spanning 19502016. Journal of Climate 30, 7801–7825. URL: https://doi.org/10.1175/JCLI-D-16-0838.1, doi:10.1175/JCLI-D-16-0838.1.

Huffman, G.J., Bolvin, D.T., Nelkin, E.J., Wolff, D.B., Adler, R.F., Gu, G., Hong, Y., Bowman, K.P., Stocker, E.F., 2007. The trmm multisatellite precipitation analysis (tmpa): Quasi-global, multiyear, combined-sensor precipitation estimates at fine scales. Journal of Hydrometeorology 8, 38–55. doi:10.1175/JHM560.1.

Jain, A.K., 2008. Data clustering: 50 years beyond k-means, in: International Conference on Pattern Recognition (ICPR), ICPR.

Jury, M.R., 2009. An intercomparison of observational, reanalysis, satellite, and coupled model data on mean rainfall in the caribbean. Journal of Hydrometeorology 10, 413–430. doi:10.1175/2008JHM1054.1.

Jury, M.R., Bernard, D., 2019. Climate trends in the east antilles islands. International Journal of Climatology 40, 36–51. URL: https://rmets.onlinelibrary.wiley.com/doi/abs/10.1002/joc.6191, doi:10.1002/joc.6191, arXiv:https://rmets.onlinelibrary.wiley.com/doi/pdf/10.1002/joc.6191.

Jury, M.R., Malmgren, B.A., 2012. Joint modes of climate variability across the inter-americas. International Journal of Climatology 32, 1033–1046.

Kaufman, L., Roussew, P.J., 1990. Finding groups in data - an introduction to cluster analysis. Journal of Applied Meteorology , 1131–1147.

Kullback, S., Leibler, R., 1951. On information and sufficiency. Annals of Mathematical Statistics 22, 79–86.

Kwitt, R., Uhl, A., 2008. Image similarity measurement by kullback-leibler divergences between complex wavelet subband statistics for texture retrieval, in: 2008 15th IEEE International Conference on Image Processing, pp. 933–936. doi:10.1109/ICIP.2008.4711909.

Lallich, S., Lenca, P., 2015. Indices de qualité en clustering, in: Journée thématique : clustering et co-clustering, Société française de classification, Issy Les Moulineaux, France.

Martinez, C., Goddard, L., Kushnir, Y., Ting, M., 2019. Seasonal climatology and dynamical mechanisms of rainfall in the caribbean. Climate Dynamics doi:10.1007/s00382-019-04616-4.

Michelangeli, P.A., Vautard, R., Legras, B., 1995. Weather regimes: Recurrence and quasi stationarity. Journal of the Atmospheric Sciences 52, 1237–1256. doi:10.1175/1520-0469(1995)052<1237:WRRAQS>2.0.CO;2.

Monteleoni, C., Schmidt, G.A., Alexander, F., Niculescu-Mizil, A., Steinhaeuser, K., Tippett, M., Banerjee, A., Blumenthal, M.B., Ganguly, A.R., Smerdon, J.E., Tedesco, M., 2013. Climate informatics. Chapman and Hall/CRC. Data Mining and Knowledge Discovery Series, pp. 81–126.

Moron, V., Frelat, R., Jean-Jeune, P.K., Gaucherel, C., 2015. Interannual and intra-annual variability of rainfall in haiti (1905–2005). Climate Dynamics 45, 915–932. doi:10.1007/s00382-014-2326-y.

Moron, V., Gouirand, I., Taylor, M., 2016. Weather types across the caribbean basin and their relationship with rainfall and sea surface temperature. Climate Dynamics 47, 601–621. doi:10.1007/s00382-015-2858-9.

Pandit, S., Gupta, S., 2011. A comparative study on distance measuring approches for clustering. International Journal of Research in Computer Science 2, 29–31.

Parmar, H., Saket, S., 2017. Overview of clustering algorithm for weather data. IJARIIE , 2395–4396.

Rokach, L., Maimom, O.Z., 2010. Clustering Methods. Springer. chapter 15. pp. 321–352.

Rousseeuw, P.J., 1987. Silhouettes: a graphical aid to the interpretation and validation of cluster analysis. Computational and Applied Mathematics 20, 5365. doi:10.1016/0377-0427(87)90125-7.

Shraddha, P., Suchita, G., 2011. Computer science and technology. computing. data processing. International journal of research in computer science , 29–31.

Sáenz, F., Durán-Quesada, A.M., 2015. A climatology of low level wind regimes over central america using a weather type classification approach. Frontiers in Earth Science 3, 15. doi:10.3389/feart.2015.00015.

Tian, W., Yuhui, Z., Yang, R., Ji, S., Wang, J., 2014. A survey on clustering based meteorological data mining. International Journal of Grid and Distributed Computing 7, 229–240.

Tibshirani, R., Walther, G., Hastie, T., 2001. Estimating the number of clusters in data set via the gap statistic. Royavl Statistic Society 5, 411–423.

Vautard, R., 1990. Multiple weather regimes over the north atlantic: Analysis of precursors and successors. Monthly Weather Review 118, 2056–2081. doi:10.1175/1520-0493(1990)118<2056:MWROTN>2.0.CO;2.

Vigaud, N., Robertson, A., 2017. Convection regimes and tropical-midlatitude interactions over the intra-american seas from may to november. International Journal of Climatology 37, 987–1000. doi:10.1002/joc.5051.

Walker, S., Damien, P., Lenk, P., 2004. On priors with a kullback-leibler property. Journal of the American Statistical Association 99, 404–408. URL: http://www.jstor.org/stable/27590396.

Xin, L., 2017. Perceptual Digital Imaging: Methods and Applications. CRC Press. volume 1. chapter Patch-Based Image Processing: From Dictionary Learning to Structural Clustering.

Yue, S., Pilon, P., Cavadias, G., 2002. Power of the mannkendall and spearman's rho tests for detecting monotonic trends in hydrological series. Journal of Hydrology 259, 254 – 271. URL: http://www.sciencedirect.com/science/article/pii/S0022169401005947, doi:https://doi.org/10.1016/S0022-1694(01)00594-7.

**Table 1**
Boundaries of the histogram classes used to quantify daily rainfall data. These edges were determined from rainfall records of the study area.

| **Centiles (%)** | 0 | 0.35 | 0.5 | 0.7 | 0.8 | 0.9 | 0.95 | 0.99 | 1 |
|---|---|---|---|---|---|---|---|---|---|
| **Rainfall (*mm*)** | 0 | ]0,1.2] | ]1.2,2.2] | ]2.2,5.2] | ]5.2,8.7] | ]8.7,16.4] | ]16.4,26.9] | ]26.9,59.2] | ]59.2,+∞[ |

**Table 2**
Descriptive statistics and probabilities: analysis of the distribution of hurricanes and tropical storms in the five clusters of the KMS-ED method. $P_{TS}(Cx)$ expresses the probability that a TS is in $Cx$, $P_H(Cx)$ expresses the probability that a H is in $Cx$, $P_{Cx}(TS)$ expresses the probability that $Cx$ produces a TS, and $P_{Cx}(H)$ expresses the probability that $Cx$ produces a H.

| **Clusters** | **TS** | **H** | **Cluster sizes** | $P_{TS}(Cx)$ | $P_H(Cx)$ | $P_{Cx}(TS)$ | $P_{Cx}(H)$ |
|---|---|---|---|---|---|---|---|
| **C1** | 1 | 12 | 799 | 0.013 | 0.049 | 0.001 | 0,015 |
| **C2** | 20 | 88 | 677 | 0.253 | 0.362 | 0.029 | 0.130 |
| **C3** | 11 | 39 | 567 | 0.139 | 0.160 | 0.019 | 0.069 |
| **C4** | 3 | 9 | 1749 | 0.038 | 0.037 | 0.002 | 0.005 |
| **C5** | 44 | 95 | 1623 | 0.557 | 0.391 | 0.027 | 0.058 |
| **Total** | 79 | 243 | 5415 | | | | |

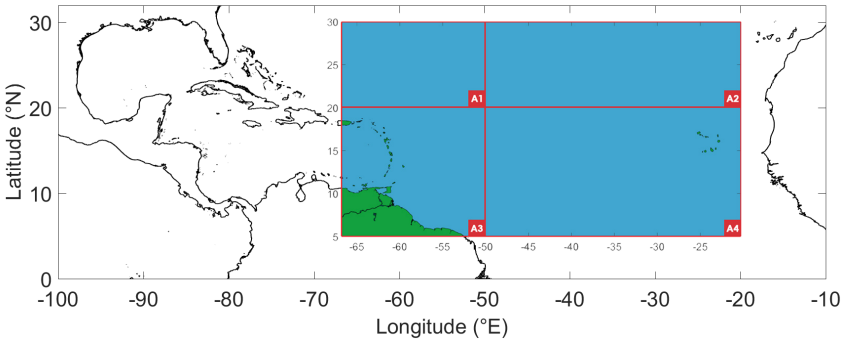


**Figure 1:** Area of interest. Land is in zone A3: Lesser Antilles with the northeasterly part of South America. Zones A1, A2, and A4 are predominantly sea: a part of the Central Atlantic Ocean and the Cape Verde archipelago. These four zones were used for the design of the expert distance (ED).

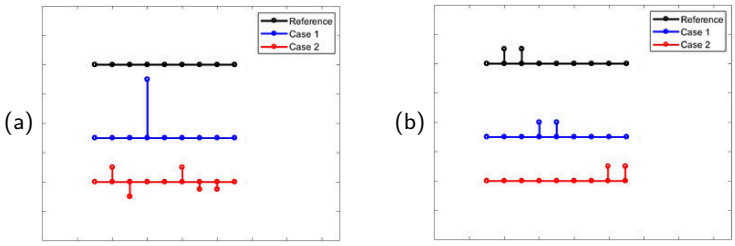


**Figure 2:** Representation of the characteristics of the L2 distance: (a) a strong and localised fluctuation (blue) produces the same L2 distance as a multitude of small variations (red) from the reference (black); (b) whether the spatial shift is low (blue) or high (red), it produces the same L2 distance from the reference (black).

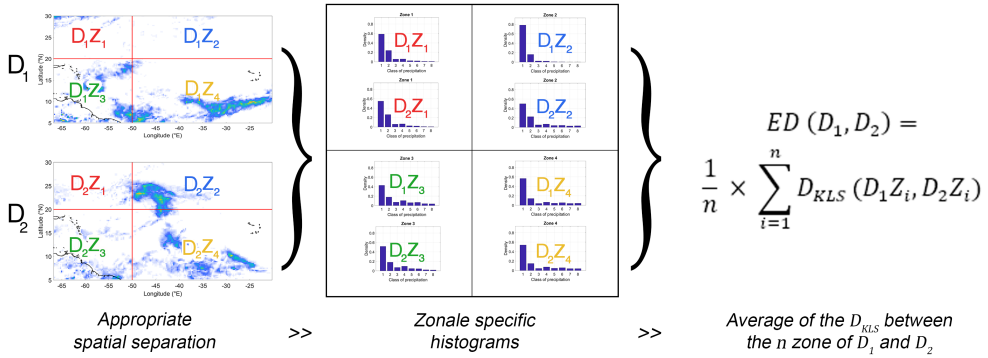


**Figure 3:** Schematic showing the computation process of the expert distance (ED) for two days $D_1$ and $D_2$: zonal quantification using custom edges ($D_xZ_i$), the use of symmetrised Kullback–Leibler divergence ($D_{KLS}$) on each zone to obtain four values, and the computation of the average to obtain $ED(D_1, D_2)$.

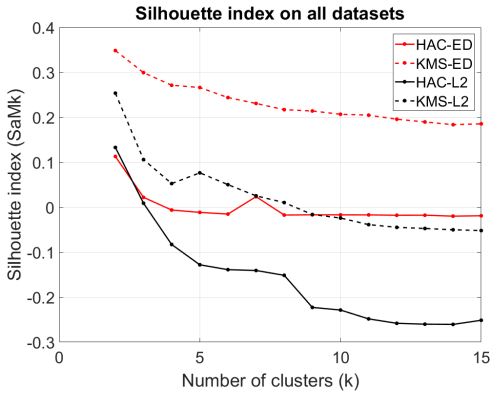


**Figure 4:** Diagram of the evolution of silhouette index ($Sa(\mathcal{M}_k)$ defined in Equation 5) in the function of $k$; the number of clusters—HAC (solid line), KMS (broken line)—using L2 (black) and ED (red).

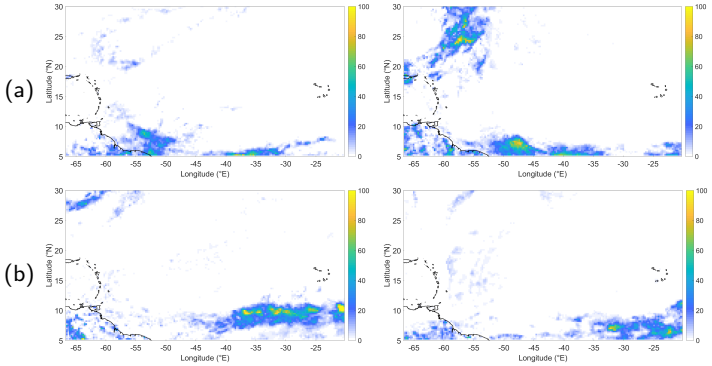


**Figure 5:** (a) Two days, for members of the same KMS-L2 cluster, but describing very different precipitation fields (TRMM), (b) Two days, for members of different KMS-L2 clusters, but very similar physically.

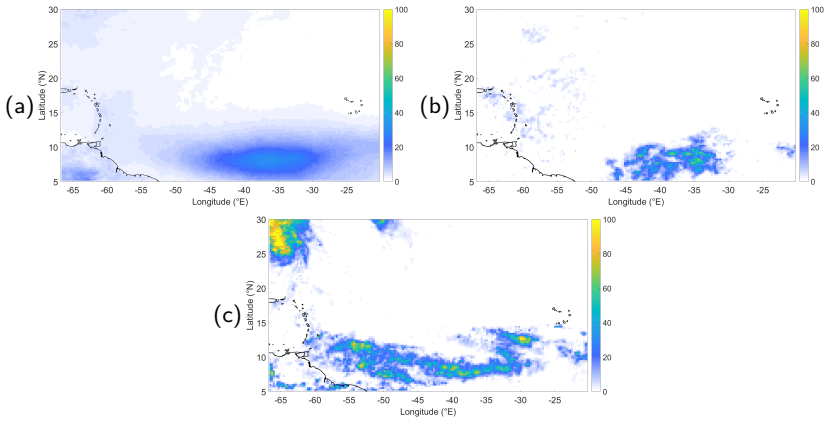


**Figure 6:** Example of the centroid of cluster C2 from *KMS-L2* computed by using the average (a) which is compared to the nearest element according to L2 (b) and another element of the cluster taken at random (c).

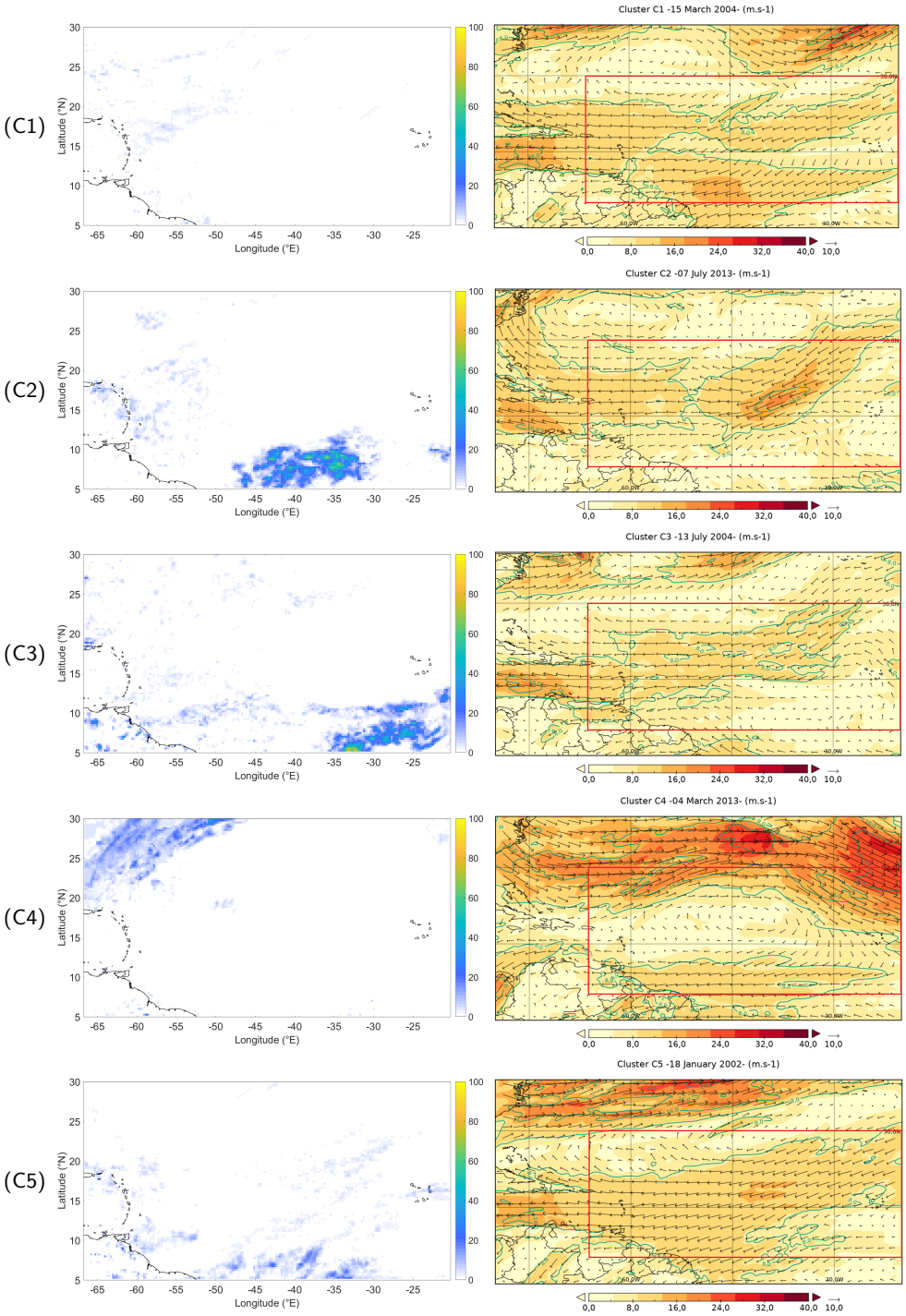


**Figure 7:** LEFT: Graph of representative elements from the KMS-L2 method, with $k = 5$, RIGHT: Graph of the wind direction and velocity from ERA-5 corresponding to the representative elements of the five clusters of the KMS-L2 method.

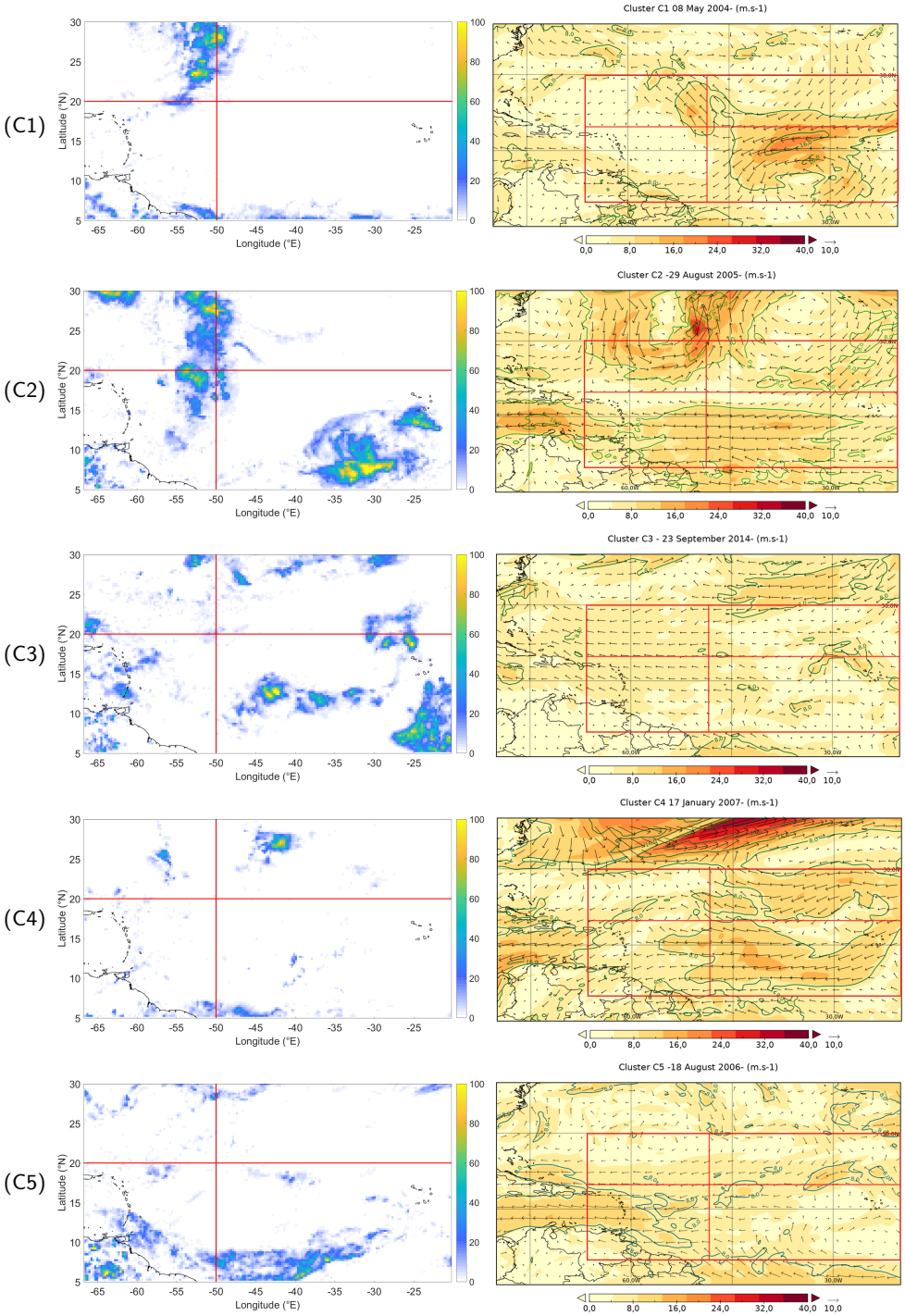


**Figure 8:** LEFT: Graph of representative elements of the clusters of TRMM rainfall from the KMS-ED method, with $k = 5$. RIGHT: Graph of the wind direction and velocity from ERA-5 corresponding to the representative elements of the five clusters of the KMS-ED method.

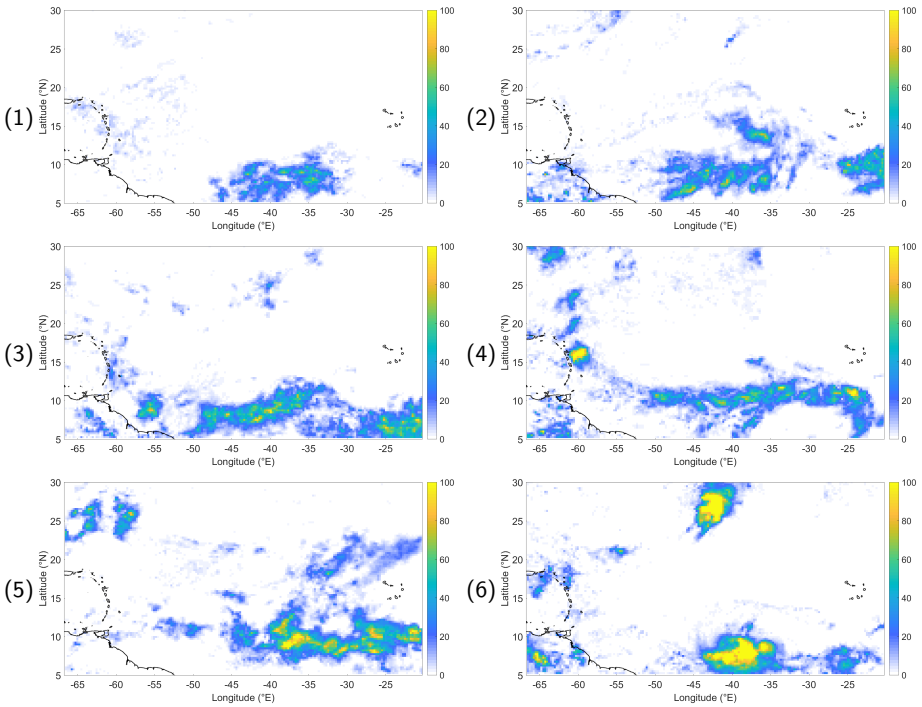


**Figure 9:** Internal variability of cluster (C2) from the *KMS-L2* method. Six days of this cluster are presented in increasing order of the L2 distance from the representative features of the cluster: (1) representative element and (2,3,4,5,6) other elements taken from a regular interval in relation to their distance L2 with (1).

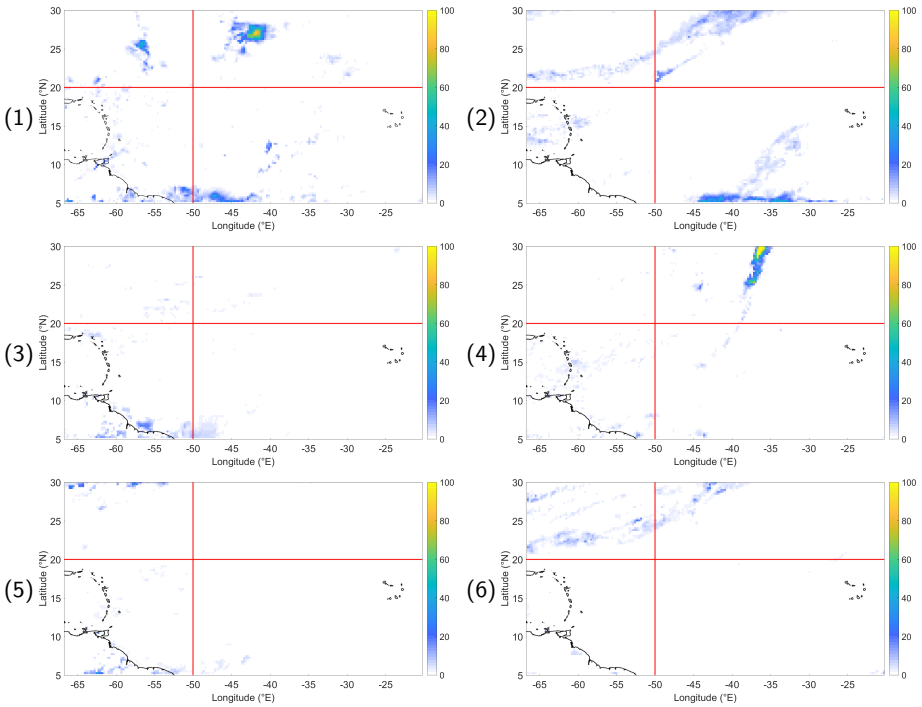


**Figure 10:** Internal variability of cluster (C4) from the *KMS-ED* method. Six days of this cluster are presented in increasing order of the L2 distance from the representative features of the cluster: (1) representative element and (2,3,4,5,6) other elements taken from a regular interval in relation to their ED with (1).

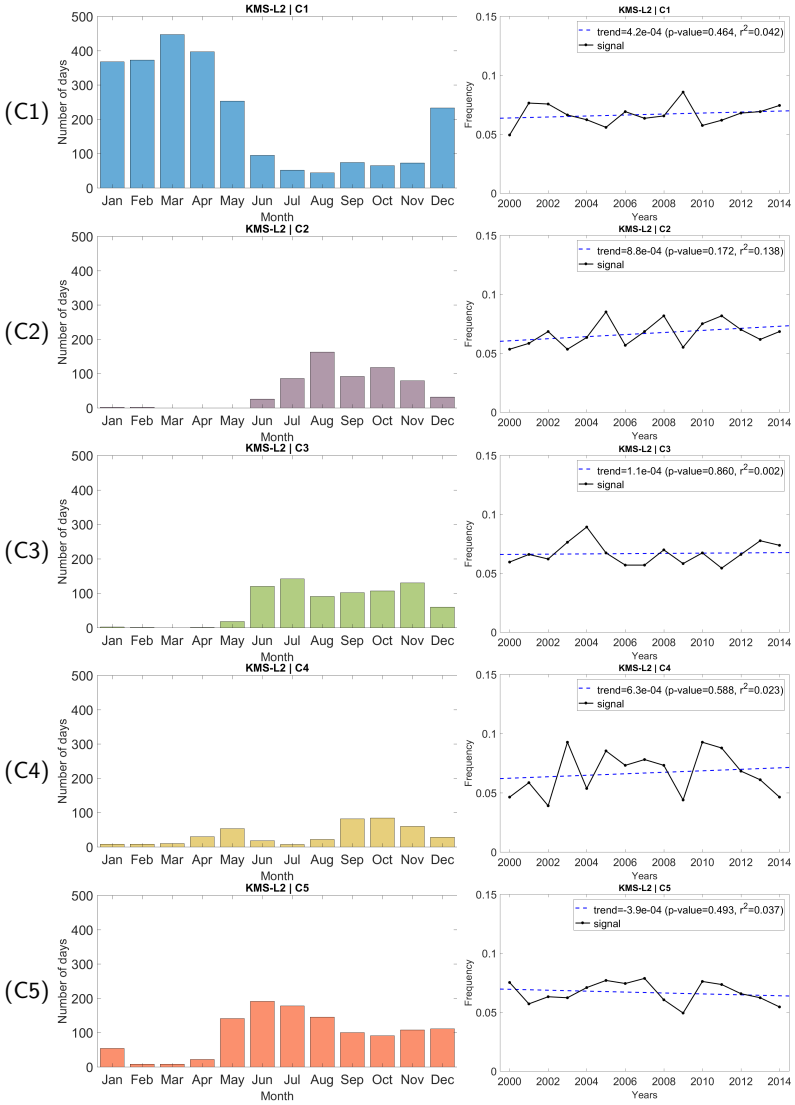


**Figure 11:** LEFT: Monthly distribution of clusters using the KMS-L2 method over the year for the period 2000 to 2014. RIGHT: Variation in the frequency of each of the clusters over the years *(with a dashed line for trends and the validity indexes)*. p-values are not statistically significant.

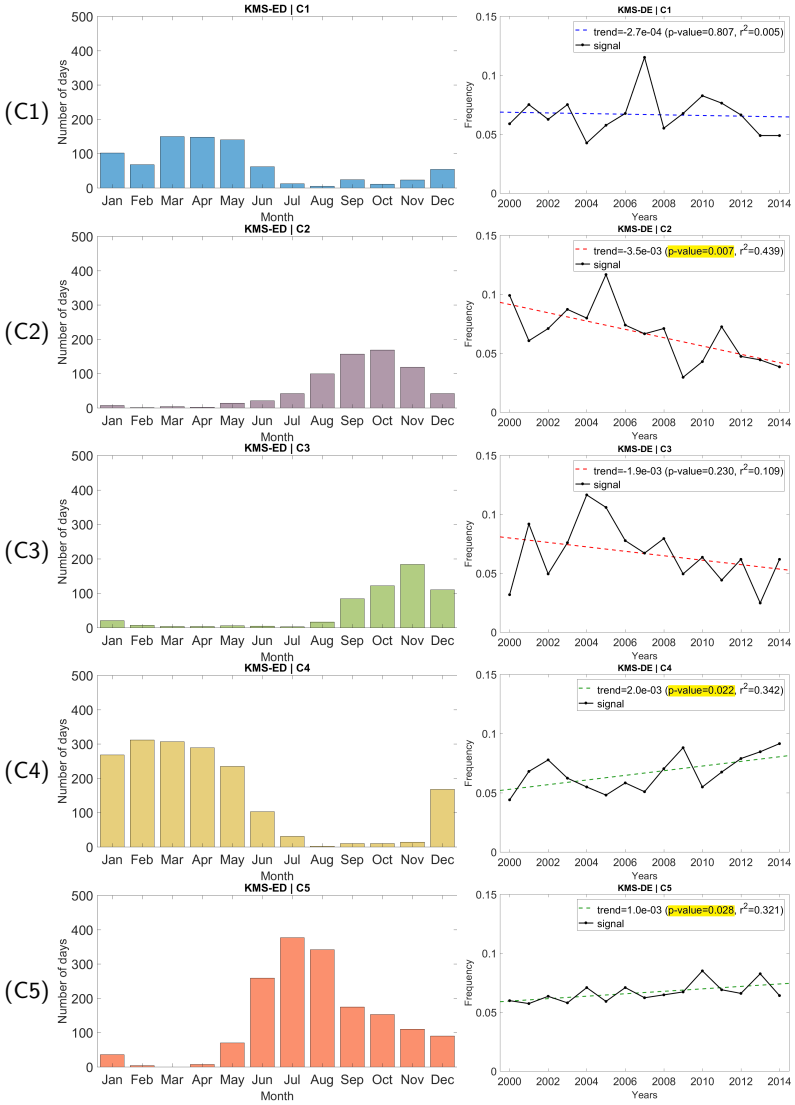


**Figure 12:** LEFT: Monthly distribution of clusters using the KMS-ED method over the year for the period 2000 to 2014. RIGHT: Variation in the frequency of each of the clusters over the years *(with a dashed line for trends and the validity indexes)*. Highlighted p-values are statistically significant ($<0.05$).

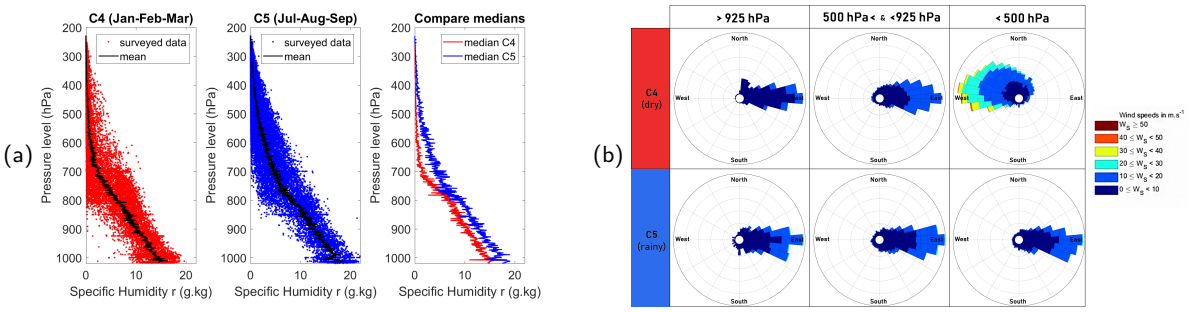


**Figure 13:** (a) Diagram of the evolution of humidity in the air layers as a function of the pressure level: the data collected by a radiosonde belonging to cluster C4 in the period January–February–March (in red) and that of cluster C5 in the period July–August–September (in blue), with their respective means (in black). (b) Diagram of the evolution of the wind direction and velocity in the air layers as a function of the pressure level: the data collected by a radiosonde belonging to cluster C4 (in red) and that of cluster C5 (in blue).

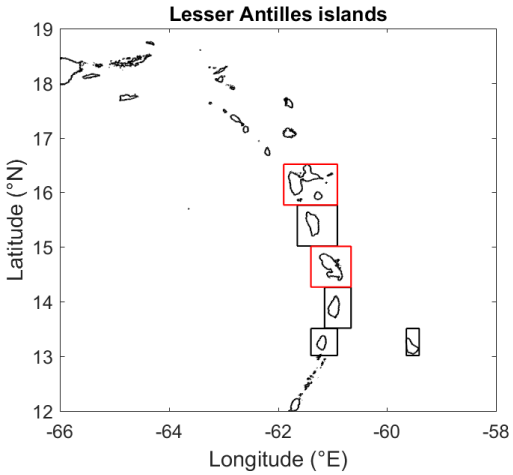


| Clusters | Infos/Islands | Guadeloupe | Dominica | Martinique | St-Lucia | Barbados | St-Vincent | Flat islands |
|---|---|---|---|---|---|---|---|---|
| C1 | **MSS** [mm/day] | 8.98 | 16.24 | 13.21 | 10.79 | 4.14 | 7.21 | 7.40 |
| | **MSM** [mm/day] | 1.50 | 1.80 | 1.47 | 1.80 | 2.07 | 1.80 | 3.38 |
| | **DWR** [%] | 37 | 39 | 34 | 43 | 57 | 50 | 34 |
| C2 | **MSS** [mm/day] | 38.68 | 57.78 | 45.88 | 33.48 | 12.12 | 24.55 | 17.49 |
| | **MSM** [mm/day] | 6.45 | 6.42 | 5.10 | 5.58 | 6.06 | 6.14 | 8.52 |
| | **DWR** [%] | 22 | 24 | 18 | 26 | 42 | 37 | 22 |
| C3 | **MSS** [mm/day] | 12.45 | 19.24 | 19.29 | 13.64 | 6.89 | 13.55 | 6.51 |
| | **MSM** [mm/day] | 2.07 | 2.14 | 2.14 | 2.27 | 3.44 | 3.39 | 3.21 |
| | **DWR** [%] | 34 | 31 | 24 | 33 | 49 | 50 | 32 |
| C4 | **MSS** [mm/day] | 6.27 | 10.67 | 9.84 | 7.40 | 4.14 | 7.31 | 3.31 |
| | **MSM** [mm/day] | 1.04 | 1.19 | 1.09 | 1.23 | 2.01 | 1.82 | 1.67 |
| | **DWR** [%] | 38 | 36 | 31 | 40 | 57 | 55 | 36 |
| C5 | **MSS** [mm/day] | 33.48 | 57.74 | 46.69 | 30.78 | 14.60 | 26.46 | 9.07 |
| | **MSM** [mm/day] | 5.58 | 6.19 | 5.19 | 5.13 | 7.30 | 6.61 | 4.65 |
| | **DWR** [%] | 24 | 21 | 14 | 19 | 41 | 35 | 27 |

**Figure 14:** UP: Lesser Antilles islands. DOWN: Detailed rainfall values measured by satellite for the Lesser Antilles islands *(with **MSS**=Mean of spatial sum [mm/day], **MSM**=Mean of spatial mean[mm/day], and **DWR**=Percentage of days without rainfall [%])*, for KMS-ED clusters (from C1 to C5).

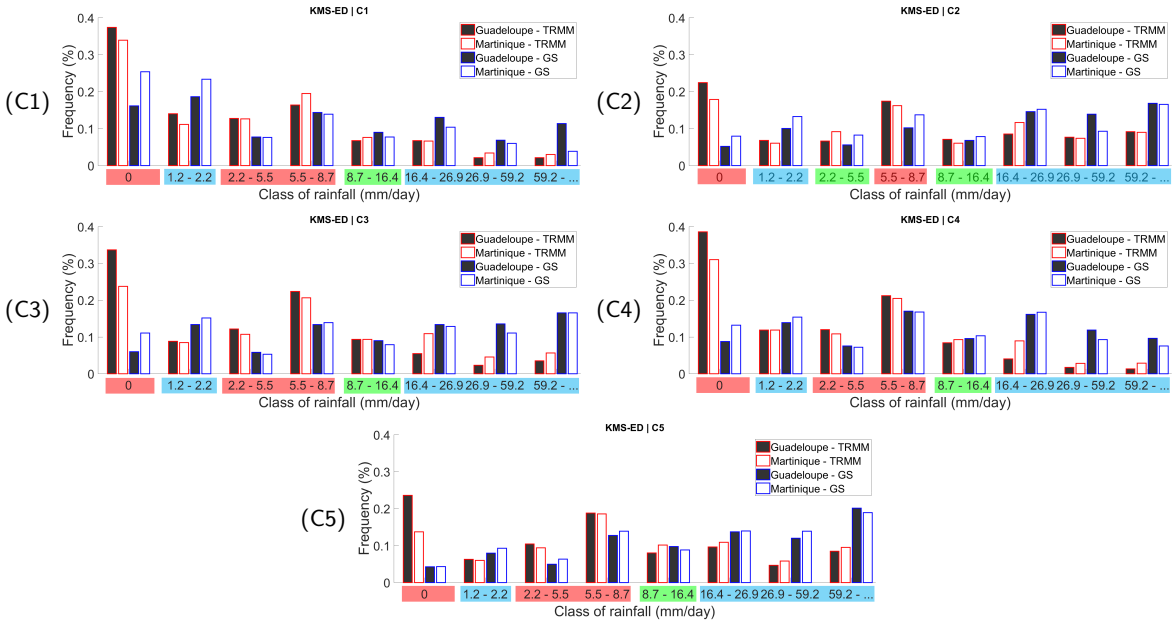


**Figure 15:** Distribution of the TRMM rainfall (red outline) compared to ground stations (GS) rainfall (blue outline) observed in Guadeloupe (in black) and Martinique (in white) for KMS-ED clusters (from C1 to C5). Classes that are overestimated by TRMM are highlighted in red, those that are underestimated are highlighted in blue, and when TRMM is nearly similar to GS, the classes are highlighted in green.

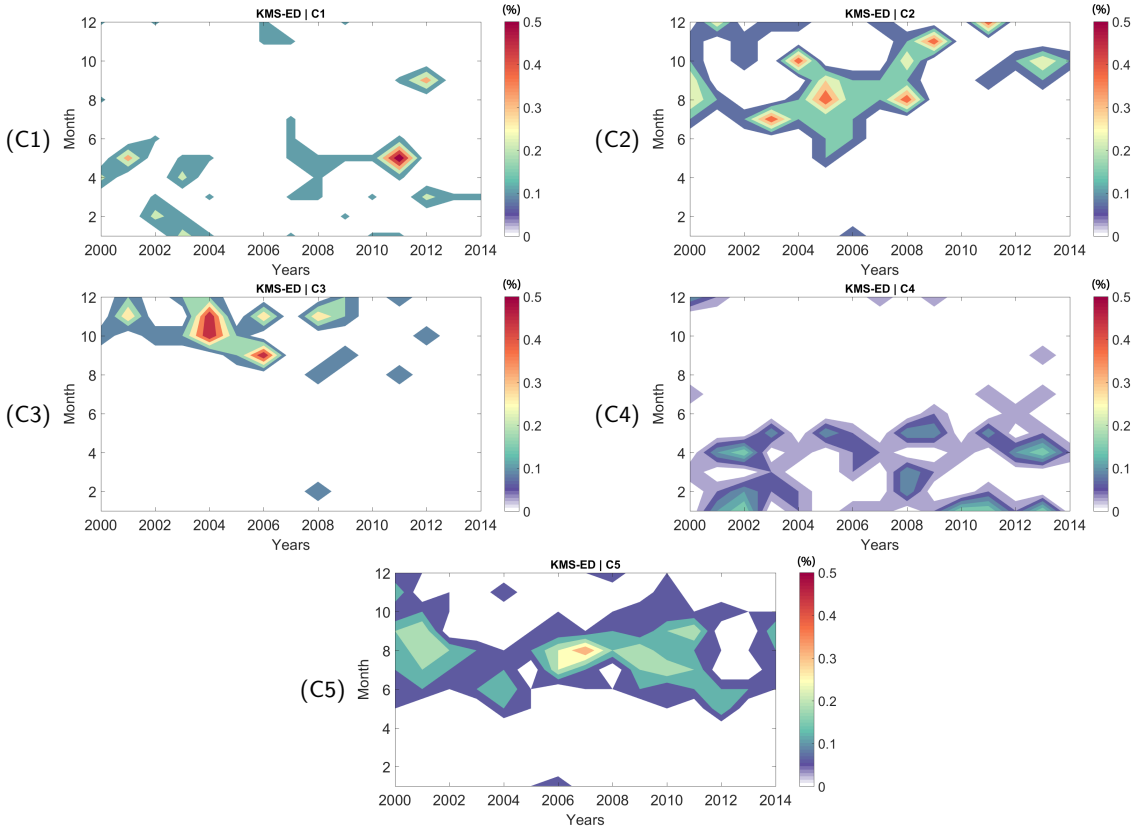


**Figure 16:** Variation in the intra-annual ($y$-axis) frequency distribution of moderate rainfall in Guadeloupe (8.7–16.4 $mm$/day) for the analysed period ($x$-axis) from 2000 to 2014 in the five different clusters of KMS-ED (from C1 to C5).

07/07/2020

09/07/2020

# Graphical Abstract

## Design of an expert distance metric for climate clustering: the case of rainfall in the Lesser Antilles

Emmanuel Biabiany,Didier C. Bernard,Vincent Page,Hélène Paugam-Moisy